Photofragmentation dynamics of hydrogen peroxide: Analysis of two simultaneously excited states

A. U. Grunewald, K.-H. Gericke, and F. J. Comes
Institut für Physikalische and Theoretische Chemie, Universität Frankfurt am Main, Niederurseler Hang, 6000 Frankfurt am Main 50, West Germany

(Received 9 June 1987; accepted 28 July 1987)

The dynamics of the photodissociation of hydrogen peroxide has been analyzed by a complete characterization of the scalar and vectorial properties of the OH fragment using Doppler and polarization spectroscopy. When hydrogen peroxide is optically excited at 193 nm the hydroxyl radicals are formed exclusively in the $X\,^2\Pi_{3/2,1/2}$ ground state with 84% of the available energy ($E_{av} = 417$ kJ/mol) being released as OH recoil translation. The remaining energy is transferred in product rotation showing a strongly inverted rotational state distribution peaking at $N'' = 12$. Vector correlations between the transition dipole moment of the parent H_2O_2 and the OH product rotational and translational motions were observed by Doppler broadened spectral lines and evaluated in terms of four bipolar moments. The quantitative contribution of two different electronic excited states in the dissociation process could be determined by analyzing the vector properties of the fragment. 62% of the OH products evolve from the $\tilde{A}\,^1A$ electronic excited state while 38% of the fragments are formed via the $\tilde{B}\,^1B$ state when hydrogen peroxide is excited at 193 nm. The OH rotational state distributions when produced from the $\tilde{A}\,^1A$ and the $\tilde{B}\,^1B$ state show no remarkable difference. The vector correlation of the recoil velocity $\mathbf{v}_{OH}$ and the rotation $\mathbf{J}_{OH}$ is strongly positive and increases with increasing J_{OH} indicating a strong preference towards $\mathbf{v}_{OH}$ and $\mathbf{J}_{OH}$ being parallel to one another. The major part of product rotation is caused by a strong dependence on the torsion angle of the two upper potential surfaces.

I. INTRODUCTION

Photodissociation dynamics provides a wealth of information in understanding chemical dynamics in general, since photofragmentation is comparable to any other molecular encounter, except that the initial conditions are very well specified. The main experimental work has concentrated on the determination of the internal state distribution of the products, e.g., the population of the electronical, vibrational, and rotational states.[1,2] A deeper insight into photodissociation processes was gained by observation of unequal population of spin and lambda doublet levels of molecular fragments of $^2\Pi$ electronic structures which are formed in the photofragmentation of H_2O,[3–5], NH_3,[6,7] HONO,[8] H_2O_2,[9–11] and R–NO.[12–15] Measurements of the recoil velocity of the products by time-of-flight[16,17] and Doppler techniques[18–20] have completed the general dynamical features of the photofragmentation process.

The obtained energy-release data describe scalar properties of the chemical interaction which can be compared directly with the results of classical or quantum scattering calculations.[4,16,21] However, even a complete knowledge of the product distribution provides only a limited view of the dissociation process, as long as vector correlations between observables are not taken into account. These correlations can be obtained by measuring Doppler profiles of the products using polarized light and different excitation and detection geometries.

The correlation between the transition dipole moment $\boldsymbol{\mu}$ in the parent and the recoil velocity vector $\mathbf{v}$ of the fragment, as well as the correlation between $\boldsymbol{\mu}$ and the rotational vector $\mathbf{J}$ of the product, may reveal the symmetry and geometry of the dissociative state.[9–15,22–28] Any decrease in fragment anisotropy of directional properties caused by parent rotation gives information on the lifetime of the parent excited state.[27–30] Very recently a substantial progress in the field of photodissociation dynamics has been achieved by observing not only the $\langle \boldsymbol{\mu} \cdot \mathbf{J} \rangle$ and $\langle \boldsymbol{\mu} \cdot \mathbf{v} \rangle$ correlation but also the correlation between the rotational and translational motion of the fragment, $\langle \mathbf{v} \cdot \mathbf{J} \rangle$, and between $\boldsymbol{\mu}$, $\mathbf{v}$, and $\mathbf{J}$.[9–13,31,32] In a triatomic molecular photodissociation the $\langle \mathbf{v} \cdot \mathbf{J} \rangle$ correlation is trivial, because the rotational vector $\mathbf{J}$ lies, in the high J limit, perpendicular to the velocity vector $\mathbf{v}$ of the diatomic fragment.[31,32] In the photodissociation of nonplanar molecules, $\mathbf{v}$ and $\mathbf{J}$ may enclose any angles and determination of $\langle \mathbf{v} \cdot \mathbf{J} \rangle$ correlation is a great help in enlightening the fragmentation process.

The additional importance of the $\langle \mathbf{v} \cdot \mathbf{J} \rangle$ correlation is its independance from the dissociation lifetime relative to the parent rotation. This correlation will persist even for predissociating states, because it is referenced only to the molecular frame and not to the LAB frame.[33,34]

In the photodissociation of H_2O_2 at 248 and 266 nm, it was found that $\mathbf{v}_{OH}$ and $\mathbf{J}_{OH}$ of the recoiling OH products are preferentially parallel to each other.[9,11] Such behavior can be explained if the torsional motion about the O–O axis is strongly involved in the fragmentation. Using the theory developed by Dixon,[33] it was possible to determine *quantitatively* the moments of the correlated angular momentum and

 0021-9606/87/225709-13$02.10

recoil velocity distribution of the OH products in the photodissociation of hydrogen peroxide at 266 nm. Such an analysis established the quantitative contribution from the vibrational motions of the H_2O_2 parent to the OH product rotation.

Observation of fragment anisotropy can also be used to discriminate between two different dissociation channels. Schmiedl *et al.*[35] have measured the $\langle \mu \cdot v \rangle$ correlation and the Doppler shift in the photodissociation of HI at 266 nm to determine the contribution of the $H + I(^2P_{1/2})$ and $H + I(^2P_{3/2})$ channels to the total fragmentation process. The analysis of the alignment and Λ doublet population of the NO product in the photodissociation of dimethylnitrosoamine at two different wavelengths was used to determine the geometry and symmetry of the first excited singlet states in the parent molecule.[15]

In this paper, we determine for the first time the quantitative contribution of two different electronic excited states in a photodissociation process of a nonplanar molecule when the parent is excited with nearly monoenergetic light. The analysis is performed by observation of Doppler broadened spectral lines and evaluation in terms of four bipolar moments. Since two electronic excited states are responsible for the dissociation process, the observed line shape is a linear combination of two Doppler profiles. The bipolar moments of the $\langle \mu \cdot v \rangle$ correlation for each contributing parent dissociation channel are used to calculate the product state distribution refering to the two different fragmentation channels. Furthermore, the dynamics of the photodissociation of H_2O_2 at 193 nm is analyzed by a complete characterization of scalar and directed properties of the recoiling OH fragments.

II. VECTOR CORRELATIONS AND DOPPLER PROFILES

Vector correlations play an increasingly important role in understanding molecular fragmentation dynamics. In the following, we will show how the vector correlation between the dipole transition moment of the parents and the translational and rotational motions of the ejected fragments can be determined by polarization and Doppler spectroscopy. In particular, the contribution of different upper potential surfaces to the total dissociation process can be extracted by knowledge of the correlation between the transition dipole of the parent and the recoil velocity of the product.

The photolysis light preferentially excites parent molecules which have a transition dipole moment parallel to the electric field vector of the dissociating radiation. This anisotropy of photoselected molecules will be transferred to the product motions if the fragmentation is fast compared with internal motions of the parent. For a diatomic parent, the direction of dissociation will only be the internuclear axis and, consequently, the angle between the E vector of the dissociating light and the recoil velocity v is either 0° for a parallel ($\mathbf{E} \| \mu \| \mathbf{v}$) or 90° for a perpendicular ($\mathbf{E} \| \mu \perp \mathbf{v}$) transition, resulting in the distributions $I(\theta) \sim \cos^2 \theta$ and $I(\theta) \sim \sin^2 \theta$, respectively. When the ejected photofragment is observed with a narrow bandwidth laser, then absorption will take place at a frequency given by $\nu = \nu_0(1 \pm v_k/c)$, where $v_k = \mathbf{k} \cdot \mathbf{v} = v \cos \theta'$ is the projection of fragment velocity v onto the direction of the probing laser beam with unit vector k. If polarization effects in detection are negligible, then the profile of each product spectral line is given by

$$g(x_D) = \frac{1}{2\Delta\nu_D}[1 + \beta P_2(\cos\theta) P_2(x_D)] , \qquad (1)$$

where $P_2(x) = (3x^2 - 1)/2$ is the second Legendre polynominal and θ describes the angle between the E vector of the dissociating laser light and the direction k of the probing laser.[33] $x_D = (\nu - \nu_0)/\Delta\nu_D$ is the ratio of displacement from line center $(\nu - \nu_0)$ to the maximum Doppler shift $\Delta\nu_D = (v/c)\nu_0$. Thus, the range of x_D is limited to $-1 \leqslant x_D \leqslant +1$. The anisotropy parameter β describes the correlation between μ, the transition dipole moment in the parent, and v, the velocity of the recoiling fragment.

If *two* different transitions are induced in the parent, i.e., two different upper electronic surfaces are populated, then the resulting Doppler profile $g(\nu)$ is nothing but a sum of two line shapes, each described by Eq. (1):

$$g(\nu) = A g_A\left(\frac{\nu - \nu_0}{\Delta\nu_D(A)}\right) + B g_B\left(\frac{\nu - \nu_0}{\Delta\nu_D(B)}\right), \quad B = 1 - A , \qquad (2)$$

where A and B are the partial contributions of the two dissociation channels to the total population of each particular quantum state. The anisotropy parameters β_A and β_B which can be extracted from the observed line profiles $g(\nu)$ give information on the symmetry and configuration of the parent excited states $\langle A |$ and $\langle B |$, if the groundstate $|X\rangle$ is known, because β_A and β_B describe the correlation between μ_A and v_A, and between μ_B and v_B, respectively ($\mu_A = \langle A | \mu | X \rangle$ and $\mu_B = \langle B | \mu | X \rangle$). When the fragments are formed with the same translational energy [$v_A = v_B$, $\Delta\nu_D(A) = \Delta\nu_D(B)$] then the individual profiles $g_A[(\nu - \nu_0)/\Delta\nu_D(A)]$ and $g_B[(\nu - \nu_0)/\Delta\nu_D(A)]$ differ only by the parameters β_A and β_B, and the observed Doppler profile is again described by Eq. (1). The parameter β in this equation is then a linear combination of β_A and β_B,

$$\beta = A\ \beta_A + (1 - A)\beta_B . \qquad (3)$$

The contribution from each dissociation channel can be obtained provided that the two anisotropy parameters β_A and β_A are known. Since the parameter β can be measured for each rotational line, the complete rotational state distribution of the product for reaction channels A and B can be determined. Therefore, very detailed information on the fragmentation process is obtained. It is still possible to describe the dissociation patterns in terms of $\langle \mu \cdot v \rangle$ correlation. However, one should keep in mind that this $\langle \mu \cdot v \rangle$ correlation represents now a sum of two (different) correlations $\langle \mu_A \cdot v \rangle$ and $\langle \mu_B \cdot v \rangle$.

Besides the correlation between the transition dipole μ of the parent and the translational motion of the fragment v, another correlation can occur between μ and J, the rotational angular momentum of the fragment. This rotational anisotropy is observed from the polarization of the chemiluminescence, provided that the product is electronically excited.[25,35,36] For fragments formed in the electronic ground state, the laser-induced fluorescence technique (LIF) is a

useful tool in determining the $\langle \mu \cdot J \rangle$ correlation from relative fluorescence intensities as a function of detection geometries and polarization of the detecting dye laser beam.[24–26]

While the translational and rotational anisotropy involve correlations in the LAB frame (simply because μ is aligned by the E vector of the dissociating photolysis light), the correlation of translational and rotational motion with *one another*, $\langle v \cdot J \rangle$, is completely independent of the LAB frame and is referenced only to the body fixed frame. Hence, rotational motion of the parent during the time of separation will not influence the $\langle v \cdot J \rangle$ correlation of the fragment.

Measurements of the $\langle v \cdot J \rangle$ correlation using Doppler spectroscopy depend only on the branch of the excitation transition and are independent of beam geometries and polarizations. To demonstrate the influence of this physical effect on the observed Doppler profiles, let us assume that there is no other correlation and that the J vector lies parallel to the velocity vector v of the recoiling fragment (Fig. 1). This positive correlation between v and J cannot occur for triatomic parent molecules fragmenting through a bent configuration, but will be caused for nonlinear polyatomic parent molecules by torsional motion about an axis parallel to the recoil direction. This was exemplarily shown in the photodissociation of H_2O_2 at 266 and 248 nm.[9,11] As will be demonstrated later, the torsional motion is a promoting mode when hydrogen peroxide is excited with radiation at 193 nm.

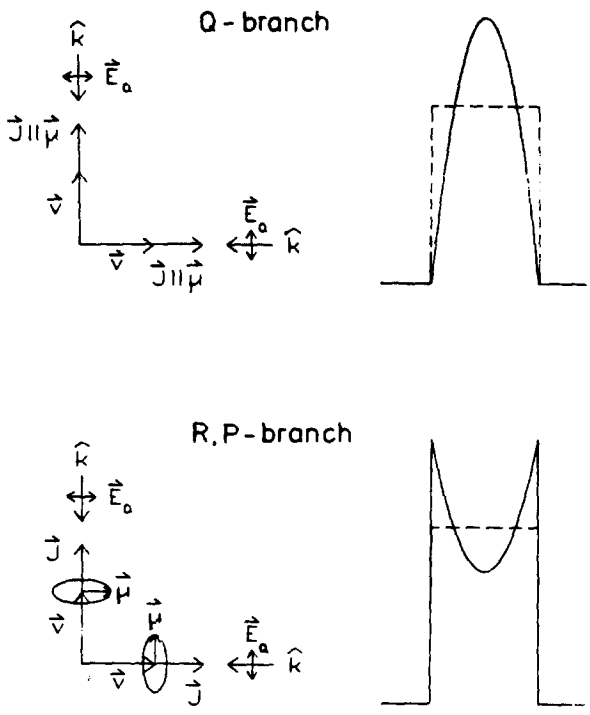

FIG. 1. Doppler profiles for uncorrelated translational motion, but with v and J being parallel to one another. When the diatomic fragment is probed via Q lines ($\mu_f \| J$), upper part of the figure, then the electric vector E_a of the analyzing beam is perpendicular to the transition dipole μ_f of the fragment for those products which absorb in the wings of the profile; while at the center of the Doppler profile, E_c and μ_f are parallel to one another. Since the probability of excitation is proportional to $|E_a \cdot \mu_f|^2$, there will be a strong reduction in absorption in the wings and substantial absorption in the center. For P or R transition, lower part of the figure, the absorption is highest with E_a perpendicular to J and thus perpendicular to v, thereby enhancing the wings of the line profile over the center.

The absorption of tunable radiation as a function of frequency should result in a rectangular Doppler profile if, there exists *no* correlation for the fragments. This behavior is described by Eq. (1) with $\beta = 0$ (dashed profile in Fig. 1). For J being parallel to v, the expected Doppler profiles for $\Delta J = 0$ and $\Delta J = \pm 1$ transitions are shown in Fig. 1.

The probability of exciting via a Q transition is highest when the electric vector E_a of the analyzing dye laser light is parallel to the rotational vector J of the fragment, because the transition dipole moment of a diatomic product lies parallel to J for $\Delta J = 0$ transitions. Since E_a is necessarily perpendicular to the photon propagation axis, those fragments which have a vanishing velocity component in direction k of the analyzing light beam exhibit a dipole moment μ_f parallel to E_a, and hence the absorption at the line center $\nu_0 (v_k = vk = 0)$ will increase in a Q transition. The other extreme would be reached by molecules which are ejected in the direction of the probing beam. The dipole moment μ_f of these fragments is perpendicular to E_a, and the absorption at the edge ($vk = v$) of the Doppler profile will vanish. Thus the observed lineprofile for a Q transition is given by the solid line if $v \| J$ (upper part in Fig. 1).

For P or R transitions, the transition dipole moment of the fragment μ_f is perpendicular to J. Therefore, the probability of excitation is highest with E_a perpendicular to J and, thus, perpendicular to v. Consequently, the absorption should increase for molecules which are ejected in the direction of the analyzing beam, thereby enhancing the wings of the line profile. The absorption at the center of the Doppler profile should decrease because this part of the line essentially represents molecules which have a transition dipole moment μ_f perpendicular to E_a. Again, the solid line represents the line profile if $v \| J$ (lower part in Fig. 1).

The above example illustrates only the effect of a positive $\langle v \cdot J \rangle$ correlation on the Doppler profile in the absence of any other correlation. In a general treatment[33,34] where $\langle \mu \cdot v \cdot J \rangle$ correlation is also included, Dixon[33] showed that the spectral line shapes for LIF detection are always a linear combination of Legendre polynominals up to order six:

$$g(x_D) = \frac{1}{2\Delta\nu_D}[g_0 + g_2 P_2(x_D) + g_4 P_4(x_D) + g_6 P_6(x_D)] . \tag{4}$$

The terms g_{k_i} itself are linear combinations of bipolar moments $\beta_0^k(k_1 k_2)$ which parameterize the μ, v, J correlations:

$$\begin{aligned} g_0 &= b_0 + b_1 \beta_0^2(02) , \\ g_2 &= b_2 \beta_0^2(20) + b_3 \beta_0^0(22) + b_4 \beta_0^2(22) + b_5 \beta_0^2(24) , \\ g_4 &= b_6 \beta_0^2(42) + b_7 \beta_0^0(44) + b_8 \beta_0^2(44) , \\ g_6 &= b_9 \beta_0^2(64) . \end{aligned} \tag{5}$$

The coefficients b_0–b_9 of these linear combinations depend on the polarization, the photolysis–detection geometry, and the branch which is used for probing the photofragments.

So far only excitation on a single upper potential surface of the parent molecule is considered. However, it is also evident that a dissociation process where several upper electronic states are involved can be characterized by a sum of different Doppler profiles described by expression (4). If repulsion on different upper potential surfaces results in different recoil velocities of the fragments, then the individual bipolar moments for each dissociation channel can be measured. For a single-fragment velocity, but different excited electronic states, the observed Doppler profile is described again by Eq. 4. However, the extracted bipolar moments $\beta_0^k(k_1k_2)$ are now positive linear combinations of bipolar moments with coefficients which determine the contribution of each upper surface to the total dissociation process.

We selected three different geometeries (II, IV, VI) for LIF analysis of the OH fragment which are related to the strongest variation of the coefficients b_i. The undispersed fluorescence is detected at right angles to both the photolysis and the analysis beam. As a typical example, the calculated values of the multipliers b_0 to b_9 of the bipolar moments are listed in Table I for three geometries and two selected transitions, $Q_1(12)$ and $P_1(12)$. The fact of observing undispersed fluorescence without a polarizer in front of the detector as well as the depolarization by hyperfine precession has been taken into account. The multipliers b_5 and b_7–b_9, which are related to g_4 and g_6 are much lower in magnitude than b_0–b_4, and consequently the influence of the corresponding moment on the observed line shapes will be negligibly small. A minor influence on the Doppler profiles could result, in principle, from the multiplier b_6. However, the higher-order moment $\beta_0^2(42)$, which is related to b_6, will tend to have a much smaller magnitude than the lower moments, unless the photodissociation process is extremely directional for $\mathbf{v}$ and $\mathbf{J}$. Furthermore, the higher terms, $P_4(x_D)$ and $P_6(x_D)$, oscillate more frequently, and thus their contribution to the line shape is averaged out by finite dye laser linewidth and Doppler broadening of the parent.

The integral of the line profile, $\int_{-1}^{+1} g(x_D)\,dx_D$, depends only on g_0. This term is related to the bipolar moment $\beta_0^2(02)$, which describes the $\langle \boldsymbol{\mu} \cdot \mathbf{J} \rangle$ correlation and is proportional to rotational alignment $A_0^{(2)}$, $\beta_0^2(02) = \frac{5}{4}A_0^{(2)}$.[9,33] The alignment of the fragments shows only an indirect influence on the shape of the absorption line and should therefore be measured in the more convenient way by monitoring the intensities of spectral lines at different polarization schemes.

TABLE I. Multipliers b_0 to b_9 of the bipolar moments for three different geometries II, IV, and VI. Depolarization by hyperfine precession has been taken into account.

Transition		$Q_1(12)$ or $^pQ_{21}(13)$			$P_1(12)$ or $^oP_{12}(13)$		
Geometry		II	IV	VI	II	IV	VI
g_0:	b_0	1.0495	0.9010	0.9010	0.9782	1.0437	1.0437
	b_1	−0.4648	0.6393	−0.3197	0.1117	−0.5156	0.2578
g_2:	b_2	−1.0495	−0.9010	1.8020	−0.9782	−1.0437	2.0874
	b_3	−1.0122	−0.7991	−0.7991	0.7488	0.6445	0.6445
	b_4	−1.2424	0.4567	0.4567	0.5875	−0.3683	−0.3683
	b_5	0.0089	0.0709	−0.0532	−0.0058	−0.0467	0.0351
g_4:	b_6	0.2346	0.6165	−0.8220	−0.2731	−0.4972	0.6629
	b_7	−0.0310	−0.0930	−0.0930	0.0204	0.0613	0.0613
	b_8	−0.0081	0.0483	0.0483	0.0053	−0.0319	−0.0319
g_6:	b_9	0.0141	0.0705	0.1410	−0.0093	−0.0465	−0.0929

The three remaining bipolar moments $\beta_0^2(20)$, $\beta_0^0(22)$, and $\beta_0^2(22)$ can be experimentally obtained by monitoring Doppler profiles at different geometries and different branches. The best method for the analysis of the vector correlations is to fit the line shapes to the function

$$g(x_D) = \frac{g_0}{2\Delta\nu_D}\left[1 + \frac{g_2}{g_0}P_2(x_D)\right]. \tag{6}$$

For each of the 12 branches, one obtains three equations (corresponding to the three different geometries II, IV, VI) to determine the bipolar moments

$$(g_2/g_0) = [b_2\beta_0^2(20) + b_3\beta_0^0(22) + b_4\beta_0^2(22)]/g_0. \tag{7}$$

The important advantage of this method is that *no* model has to be assumed for the fragmentation process, because the moments of the correlated transition dipole moment, the angular momentum, and the recoil velocity can be obtained by straightforward "inversion" of observed Doppler profiles.

The bipolar moment $\beta_0^2(20) = \langle P_2(\cos\theta_t)\rangle$ in Eq. (5) describes the correlation between $\boldsymbol{\mu}$ and $\mathbf{v}$ and is proportional to the conventional translational anisotropy parameter β in Eq. (1), $\beta_0^2(20) = \frac{1}{2}\beta$. If several upper electronic states are involved in the fragmentation process, the contribution of each dissociation channel can be obtained from the observed bipolar moment $\beta_0^2(20)$, provided the "individual" bipolar moments of each single fragmentation channel are known [see Eqs. (2) and (3)].

The $\langle \mathbf{v} \cdot \mathbf{J} \rangle$ correlation of the fragment is given by the moment $\beta_0^0(22) = \langle P_2(\cos\theta_{tr})\rangle$. The spherical symmetry of this moment implies that the $\langle \mathbf{v} \cdot \mathbf{J} \rangle$ correlation will be observed independent of the rotation of parent molecule. In the high J limit, the numerical range of this moment lies between $-1/2$, when $\mathbf{J}$ is perpendicular to $\mathbf{v}$ and $+1$, when $\mathbf{J}$ is parallel to $\mathbf{v}$.

The bipolar moment $\beta_0^2(22)$ describes the mutual correlation between the parent transition dipole $\boldsymbol{\mu}$ and the translational $\mathbf{v}$ and rotational $\mathbf{J}$ motion of the fragment. The limiting numerical value will be -1 when $\boldsymbol{\mu}$, $\mathbf{v}$, and $\mathbf{J}$ are all perpendicular to one another or pointing all in the same direction. In the case where two of the three vectors are parallel to one another but perpendicular to the third, $\beta_0^2(22)$ reaches the other limiting value of $+1/2$. Usually one expects a low value of $\beta_0^2(22)$ becasue (i) it is unlikely that the photolysis results in an anisotropic distribution which is extremely directional for both $\mathbf{v}$ and $\mathbf{J}$ relative to $\boldsymbol{\mu}$ and (ii) this bipolar moment is the most sensitive to motion of the parent before fragmentation.

So far, we neglected only terms higher than $P_2(x_D)$ in Eq. (4), but made the assumption of a single recoil velocity, an infinite small laser linewidth, and a negligible parent thermal translational motion. For a center of mass recoil velocity distribution $f(v)$ of products, the corresponding photofragment Doppler profile is described by[19]

$$g(v_k) = \int_{v_k}^{\infty} \frac{f(v)g_0}{2v}\left[1 + (g_2/g_0)P_2\left(\frac{v_k}{v}\right)\right]dv. \tag{8}$$

This function has to be convoluted with the parent velocity distribution and laser line shape to obtain an expression which has to be fitted to the observed Doppler profiles.

The photodissociation of hydrogen peroxide at 193 nm yields OH fragments with a very narrow rotational state distribution and no vibrational excitation. Thus, the spread in product velocity has to be very small and only the translational motion and the limited spectral resolution of the measurement have to be considered. The laser line was found to be well represented by a Gaussian profile with a width of $\Delta\nu_l = 0.095\ \mathrm{cm}^{-1}$ (FWHM). The combination with the parent Gaussian distribution ($\Delta\nu_{H_2O_2} = 0.069\ \mathrm{cm}^{-1}$) at a temperature $T = 300$ K gives the overall Gaussian convolution function for the analyzing dye laser with a width of $\Delta\nu_a = 0.12\ \mathrm{cm}^{-1}$ (FWHM).

A least square fit procedure to the expression

$$D(\nu_a,\nu_0) = A\int_{\nu_0-\Delta\nu_D}^{\nu_0+\nu_D} \exp\left[-4\ln 2\left(\frac{\nu-\nu_a}{\Delta\nu_a}\right)^2\right] \times\left[1-(g_2/g_0)P_2\left(\frac{\nu_0-\nu}{\Delta\nu_D}\right)\right]d\nu + B\,, \qquad (9)$$

where ν_a represents the frequency of the analyzing dye laser, yields background (B), amplitude (A), doppler shift ($\Delta\nu_D$), and the ratio (g_2/g_0) which represents the bipolar moments described above.

III. EXPERIMENTAL

The basic experimental set up is shown in Fig. 2. The reaction chamber is made of stainless steel and evacuated by two 500 ℓ/s oil diffusion pumps. The vessel is provided with two gas inlet systems allowing observation of the photodissociation process in the bulk as well as in the supersonic jet. In the present study the probe gas is continuously flowing at low pressures through the cell. The H_2O_2 solution used in the experiment is 95% pure and stored in a glass bulb. Gas flow and pressure can be regulated by a glass needle valve. To guarantee that a photoproduct formed in a particular quantum state is not disturbed by subsequent collisions during the time of interrogation, the reaction chamber pressure is decreased until the product state distribution remains unchanged. In all following investigations the total chamber pressure was set to ~ 0.65 Pa where no relaxation processes can be observed.

The H_2O_2 molecules were photolyzed by an ArF laser. Its radiation was polarized by a Rochon prism. The polarization direction $\mathbf{E}_P$ is adjustable by rotation of the prism. The photolysis beam was unfocused but collimated outside the vacuum chamber to a spot size of ~ 3.5 mm diameter. Product states distributions and Doppler profiles were probed by laser induced fluorescence (LIF). Resonant fragment excitation was performed by a frequency doubled tunable dye laser (Lambda Physik Fℓ] 2002; Inrad autotracking system) pumped by the second harmonic of a Nd:YAG laser (Spectron SL2Q). To obtain a wide tuning range with an optimum of constant output energy, a mixture of DCM and rhodamine B dye solutions was used. The integrated OH absorption line intensities were determined using a dye laser linewidth in the UV of 0.5 cm^{-1} (FWHM). For Doppler line shape recording, the linewidth was narrowed by an intracavity étalon to 0.095 cm^{-1} (FWHM). Scanning of the dye laser was controlled by a 16 bit microcomputer.

A half-wave retardation plate gives the possibility to turn the plane of the electric vector $\mathbf{E}_a$ by 90°. The dye laser beam was carefully adjusted to overlap with the photolysis beam in the middle of the cell. Background noise, due to scattered laser light in the vacuum chamber was reduced by four baffled arms mounted at the cell. The experiment was performed under mutually orthogonal geometry (Fig. 3). The advantage of this arrangement is the possibility to realize three geometries with significant different influence on the recorded Doppler line shape of anisotropic fragment distribution without changing the beam path, but only the polarization vectors $\mathbf{E}_P$ and $\mathbf{E}_a$. The same assignment for the geometries as in Ref. 9 is used for a better comparison.

The LIF signal was viewed perpendicular to the plane formed by the two laser beams with a photomultiplier tube (bialkali) equipped with an imaging optics and an interference filter (310 ± 10 nm), but without the use of polarizers. The pulse energies of the lasers were monitored by two pyro-

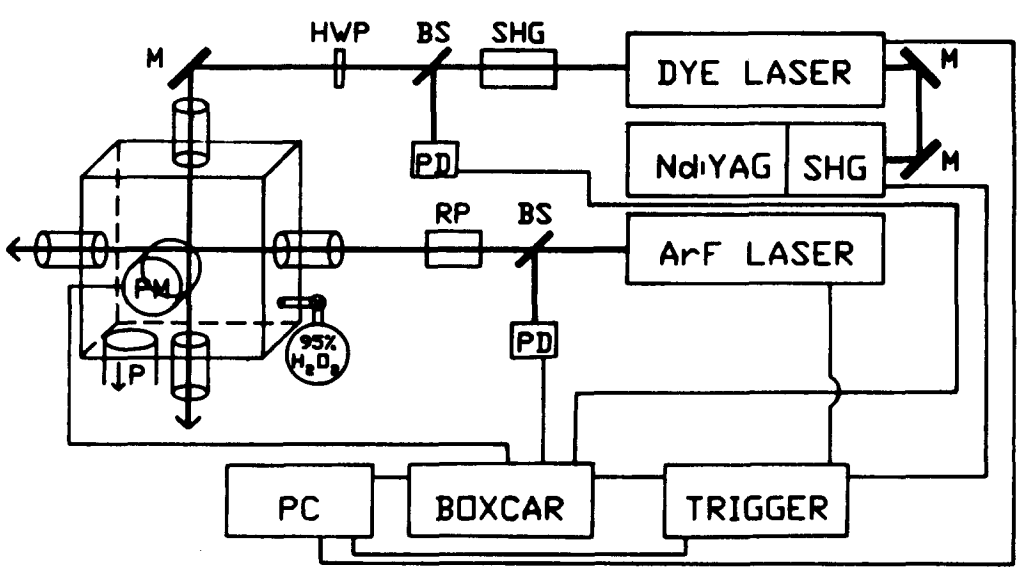

FIG. 2. Schematic diagram of the experimental setup.

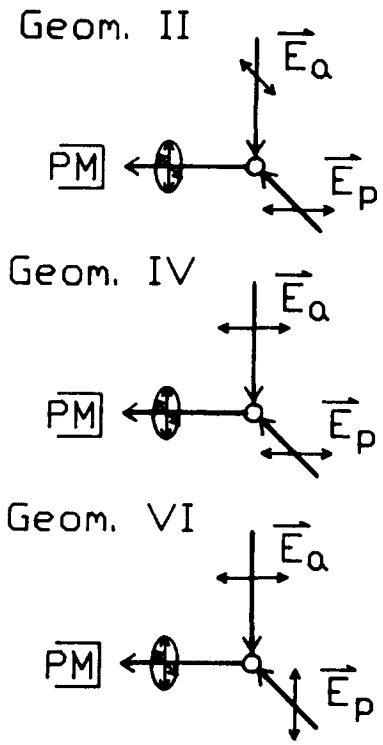

FIG. 3. Characterization of the three different photolysis analysis detection geometries (II, IV, VI) used to determine the vector correlations in the photofragmentation process of hydrogen peroxide at 193 nm.

electric detectors. The photomultiplier output voltage and the detector signals were measured with a three channel boxcar integrator (Stanford, SRS 250) and stored after A/D conversion in the microcomputer, which normalized the fluorescence signal to the photolysis and probe laser energies on a shot to shot basis.

A homemade trigger device controlled all time events in the experiment. The delay between the ArF and dye laser was set to 50 ns for best S/N ratio. The gate duration was 1 μs placed 50 ns after the probe laser pulse. In an investigation of vector correlations, saturation must be avoided in the detection of fragment as well as in the excitation of parent molecules because the photoselection of the molecules with linear polarized light must be assured. The linear dependence of the fluorescence signal on both the photolyzing and the analyzing laser pulse energies was proved to be valid for the applied energies of $\sim 5\,\mu$J for product and ca. 5 mJ for parent excitation.

IV. RESULTS

In the absorption spectrum of hydrogen peroxide, the excitation wavelength of 193 nm is near the maximum of the first UV absorption continuum.[37] Since the absorption contour is smooth without any structure, one expects a prompt dissociation process. It could be shown that the lowest electronical excited state is of ^1A symmetry, arising from the promotion of one of the two ($4b$) electrons to the lowest antibonding $5b$ orbital.[28,38] On excitation of the $\tilde{A}\,^1A$ state, hydrogen peroxide dissociates in less than 60 fs.[9,11] Radiation at 266 and 248 nm excites H_2O_2 only to this ^1A state, but the much shorter wavelength of 193 nm can also induce a transition to the $\tilde{B}\,^1B$ state.

Ondrey *et al.* supposed that at 193 nm several upper surfaces may be responsible for the absorption, because a bimodal rotational state distribution for OH products was found.[39] However, the observed distribution is not nascent in character, but is perturbed by fast rotational relaxation.[10] The *nascent* rotational state distribution is strongly non-Boltzmann-like and can be described by a Gaussian-type function with a maximum at the quantum number $N''_{OH} = 12$.

Independent of the number of hypersurfaces involved in the photolysis of a molecule, the fragmentation process can always be analyzed by Doppler and polarization spectroscopy provided the fragments exhibit a suitable transition. If several excited states lead to the rupture of a bond, then the quantitative contribution of each reaction channel can be obtained from the observed $\langle \mu \cdot v \rangle$ correlation, parameterized by the bipolar moment $\beta^2_0(20)$.

A. OH rotational alignment

The OH product distribution in the $v'' = 0$ level is probed by excitation of the $X\,^2\Pi(v''=0) \rightarrow A\,^2\Sigma^+(v'=0)$ band and by detection of the undispersed fluorescence. The populations $P(q'')$ of photofragments formed in the quantum state q'' can be deduced from the measured intensities I of the LIF spectrum using the expression

$$I = CB(q'',q')\nu P(q'')\,[b_0 + b_1 \beta^2_0(02)], \qquad (10)$$

where C is a constant, ν is the excitation frequency, and $B(q'',q')$ are the tabulated B coefficients for absorption. The bracket term describes the angular dependence of the fluorescence signal and contains the molecular alignment $\beta^2_0(02) = \frac{5}{4}A^{(2)}_0$. Thus, one has to know the correlation between fragment angular momentum and polarization direction of the photolyzing light to deduce reliable product state populations.

The bipolar moment $\beta^2_0(02)$ was obtained by determining the ratio of the relative P/Q branch intensities for the two different geometries IV and VI ($\mathbf{E}_p \| \mathbf{E}_a$ and $\mathbf{E}_p \perp \mathbf{E}_a$). It should be mentioned that the two laser beams require a careful adjustment to avoid variations in the line intensities at the two geometries, because differences in intensities can be misinterpreted as rotational alignment of the photofragments. In the high J limit, the range of the moment is limited to $-\frac{1}{2} \leqslant \beta^2_0(02) \leqslant +1$, corresponding to fragment rotation parallel or perpendicular to the transition dipole moment of the parent.

In the photodissociation of H_2O_2 at 193 nm, no effect of OH alignment on the intensities could be observed. Any variation of $\beta^2_0(02)$ as function of OH rotation is within the experimental scatter, $\beta^2_0(02) = 0.00 \pm 0.05$. Since there is no $\langle \mu_{H_2O_2} \cdot J_{OH} \rangle$ correlation, the line intensities can be directly converted into product state distributions.

B. Internal state distribution

The relative population number of each quantum state was usually taken from the P and Q main lines. The origin of the P branch is the Π^+ component, while the Q branch probes the Π^- component. In general, Π^- is higher in energy than the Π^+ component. Only for the four lowest rotational levels of the $^2\Pi_{1/2}$ system is the energetic ordering reversed. The ratio of the relative Λ doublet population R_Λ

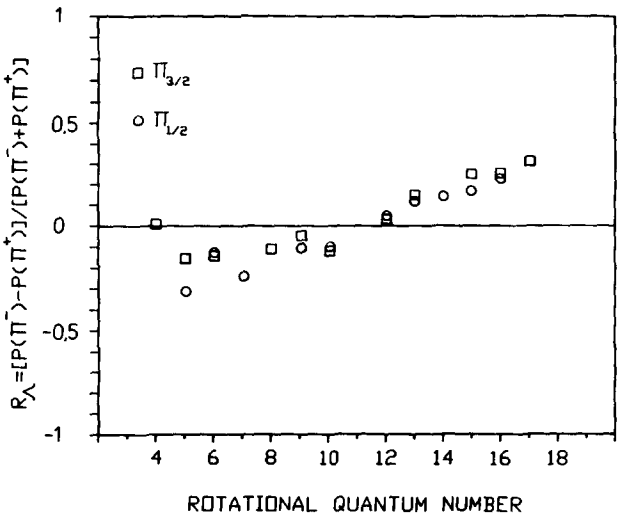

FIG. 4. Distribution of the two Λ doublets Π^+ and Π^- as a function of N''_{OH} for the $^2\Pi_{3/2}$ system after photodissociation of hydrogen peroxide at 193 nm. The population of the components Π^+ and Π^- component are probed by P and Q lines, respectively.

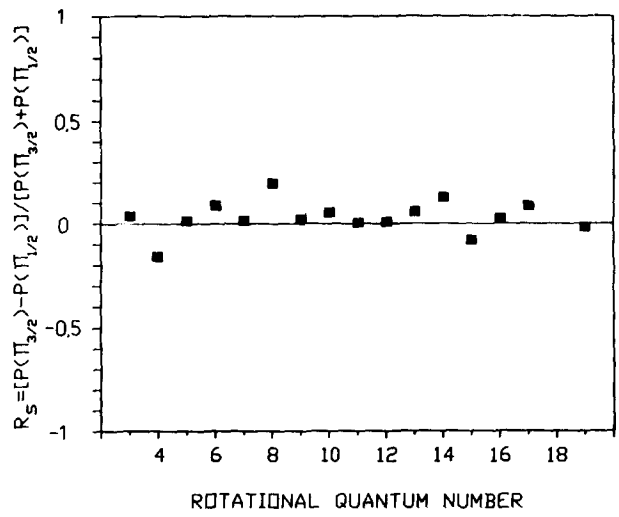

FIG. 5. Product state distribution of the spin components $^2\Pi_{3/2}$ and $^2\Pi_{1/2}$ as a function of N''_{OH}. The different statistical weights have been taken into account. The horizontal line at $R_S = 0$ indicates that the dissociation process does not distinguish between the two spin–orbit states.

$= [P(\Pi^-) - P(\Pi^+)]/[P(\Pi^-) + P(\Pi^+)]$ as a function of the angular momentum N''_{OH} of the OH fragment is shown in Fig. 4. For $R_\Lambda = 0$, a statistical population between the two Λ components is expected. We observe a slightly negative value for low rotational states indicating a preference for the Π^+ state; while for $N''_{OH} \geqslant 10$, a small population inversion between the Λ components was found. This preferential population of the Π^- Λ doublet increases with increasing OH fragment rotation.

In the high J limit, the $p\pi$ lobe of the unpaired electron is aligned parallel to the rotational vector **J** for the Π^- component and perpendicular to **J** for the Π^+ component. The observed nonstatistical population of the Λ doublet is well below the value found in many simple systems, such as H_2O^3 or HONO,[8] and the single occupied $p\pi$ orbital does not reach the maximum possible alignment.

The influence of the electron spin in the photodissociation of H_2O_2 at 193 nm has been analyzed by calculating the ratio $R_S = [P(^2\Pi_{3/2}) - P(^2\Pi_{1/2})]/[P(^2\Pi_{3/2}) + P(\Pi_{1/2})]$ where $P(^2\Pi_1)$ represents the population numbers of the $^2\Pi_{3/2}$ or $^2\Pi_{1/2}$ state (Fig. 5). No significant deviation from a line parallel to the abscissa with the intercept at $R_S = 0$ is observed. Therefore, the population is distributed statistically between the two spin components, and, hence, the fragmentation process does not distinguish between the two spin-orbit states, $^2\Pi_{3/2}$ and $^2\Pi_{1/2}$.

The total energy release available for excitation of the two OH($X\,^2\Pi$) photoproducts is $E_{av} = 416.9$ kJ/mol, of which 16% (33.3 kJ/mol for each one of the two OH fragments) is transferred into product rotation with a Gaussian-type distribution over the various rotational states. Since no vibrationally excited OH fragments are observed, the remaining 84% of the excess energy is released into fragment recoil translation.[10] Therefore, the dynamics of the fragmentation process is dominated by strong repulsion along the O–O bond, and photoproducts with a high recoil velocity but narrow velocity distribution are expected. The most probable OH velocity is determined by $v_{OH} = (0.84\, E_{av}/m_{OH})^{1/2} = 4540$ ms^{-1} corresponding to a Doppler shift of ~ 0.49 cm^{-1}. Since the probe laser linewidth as well as the parent Doppler motion is small compared to this OH Doppler shift, it is possible to examine the various vector correlations by line profile measurements.

C. Translational anisotropy

The anisotropic fragmentation patterns were extracted by observation of recoil Doppler broadened line profiles at three different geometries for OH product rotations between $N''_{OH} = 4$ and $N''_{OH} = 18$. The population of lower or higher rotational states is extremely small and negligible in the overall mechanism of the photodissociation process of hydrogen peroxide at 193 nm.

As an example, the line profiles for the $Q_1(12)$ (geometry IV), $R_1(4)$ (geometry VI), and $P_1(12)$ (geometries IV and VI) transitions are shown in Fig. 6. The Doppler profiles were fitted to the expression (9) in a least squares fit procedure and the profile obtained are shown in this figure as a solid smooth curve. The line shapes are not only sensitive to the product translational anisotropy but also to a correlation of the translational and rotational motion of the fragment. The influence of this $\langle \mathbf{v}_{OH} \cdot \mathbf{J}_{OH} \rangle$ correlation on the observed Doppler profile is elucidated in the next section. Observation of the translational anisotropy is extremely sensitive to a change in geometries ($\mathbf{E}_p \| \mathbf{k}$ or $\mathbf{E}_p \perp \mathbf{k}$). The observed line shapes show only a minor influence when the electric vector $\mathbf{E}_p$ of the photolysis laser light is turned from a perpendicular (geometry IV) to a parallel orientation (geometry VI) relative to the beam direction of the analyzing dye laser (lower part of Fig. 6). Therefore, the angular dis-

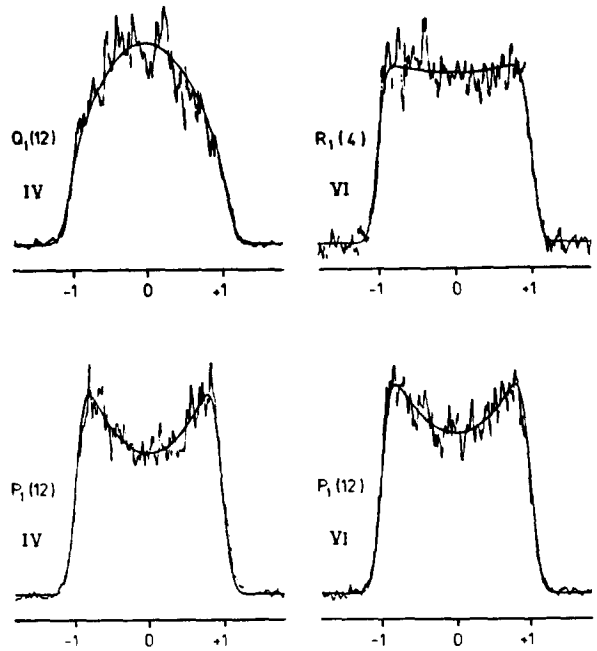

FIG. 6. Recoil–Doppler broadened line profiles of the $Q_1(12)$, $P_1(12)$, and $R_1(4)$ transitions at the two different geometries IV and VI. Only a minor difference in the line shapes for the $P_1(12)$ transition at geometry IV and VI was observed. Thus, the overall translational anisotropy must be very small. The central dip of the $P_1(12)$ transition in contrast to the rounded profile of the $Q_1(12)$ transition indicates a strong parallel orientation of $\mathbf{J}_{OH}$ to $\mathbf{v}_{OH}$. At low OH rotational quantum numbers, the profiles become more flat indicating a decreasing $\langle \mathbf{v}_{OH} \cdot \mathbf{J}_{OH} \rangle$ correlation.

tribution of OH photoproducts is nearly isotropic about the electric vector of the dissociating radiation.

In Figs. 7(a)–7(c), the bipolar moments $\beta^2_0(20)$, $\beta^0_0(22)$, and $\beta^2_0(22)$ evaluated according to the procedure described in Sec. II, are plotted as a function of the rotational motion of OH. The moment $\beta^2_0(20)$ which is proportional to the conventional defined anisotropy parameter $\beta = 2\beta^2_0(20)$, is shown in Fig. 7(a). $\beta^2_0(20)$ contains information on the symmetry, configuration, parent internal motion, and on the lifetime of the parent excited state. If different electronic excited states are involved in the fragmentation process, then the value of $\beta^2_0(20)$ reflects the quantitative contribution of each excited surface.

D. Correlation between v_{OH} and J_{OH}

The mutual correlation of the photofragment translational and rotational vectors $\mathbf{v}_{OH}$ and $\mathbf{J}_{OH}$ is described by the bipolar moment $\beta^0_0(22)$ and is independent of the frame of reference. The strong positive correlation between $\mathbf{v}_{OH}$ and $\mathbf{J}_{OH}$ is demonstrated in Fig. 6 for the $Q_1(12)$ and $P_1(12)$ transitions. The deep central dip in the recoil broadened Doppler profile for the P line vanishes when the same rotational state is probed by a Q transition. Since the probability of excitation via Q transitions is highest when the electric vector $\mathbf{E}_a$ of the analyzing light is parallel to $\mathbf{J}_{OH}$, the recoil velocity vector $\mathbf{v}_{OH}$ must also lie more parallel to $\mathbf{J}_{OH}$.

The central dip in the line shapes is less significant when lower rotational states are probed by P or R lines (see Fig. 6, $R_1(4)$ transition). Therefore, one expects a less positive

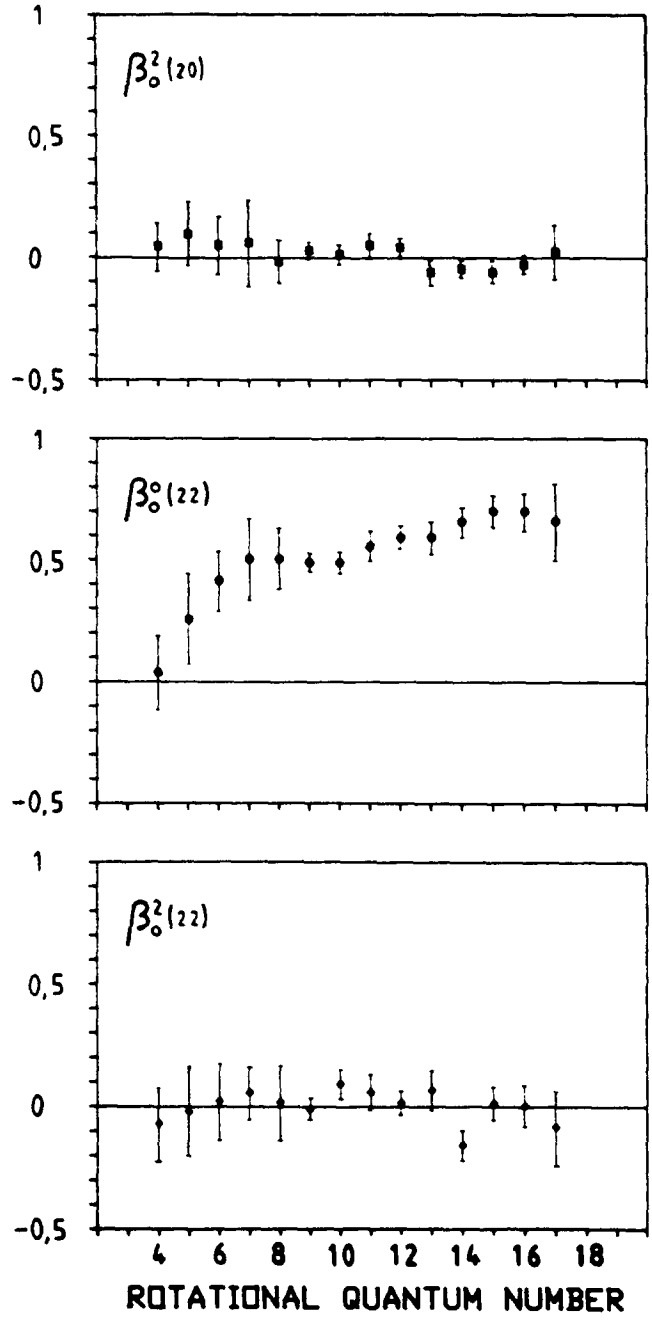

FIG. 7. The observed bipolar moments $\beta^2_0(20)$, $\beta^0_0(22)$, and $\beta^2_0(22)$ as a function of N''_{OH}. The parameter $\beta^2_0(20)$ characterizes the translational anisotropy of photofragments. The value is used to determine the quantitative contribution of the $\tilde{A}\,^1A$ and $\tilde{B}\,^1B$ electronic excited states to the overall dissociation process. The bipolar moment $\beta^0_0(22)$ is positive and increases with increasing product rotation indicating a more parallel orientation of $\mathbf{J}_{OH}$ to $\mathbf{v}_{OH}$, independent of the microscopic dissociation channels ($\tilde{A}\,^1A$ or $\tilde{B}\,^1B$) involved in the fragmentation process. The bipolar moment $\beta^2_0(22)$ describes the correlation of the transition dipole moment $\mu_{H_2O_2}$ of the parent with the translational and rotational motion of the OH product. Its low value close to zero is a consequence of the low value for the translational anisotropic parameter $\beta = \frac{1}{2}\beta^2_0(20)$ and the alignment $A^{(2)}_0 = \frac{1}{5}\beta^2_0(02)$.

$\langle \mathbf{v}_{OH} \cdot \mathbf{J}_{OH} \rangle$ correlation for lower rotations of the OH fragment. A quantitative description of the $\langle \mathbf{v}_{OH} \cdot \mathbf{J}_{OH} \rangle$ correlation is given by the bipolar moment $\beta^0_0(22)$, and its dependence on the OH rotation is shown in Fig. 7(b). For low

rotational quantum numbers, the value of the bipolar moment is close to zero, but slightly positive, still indicating a more parallel orientation between $\mathbf{v}_{OH}$ and $\mathbf{J}_{OH}$. With increasing N''_{OH}, the positive $\langle \mathbf{v}_{OH} \cdot \mathbf{J}_{OH} \rangle$ correlation increases, and for high OH rotational states ($N''_{OH} > 12$) we obtain a value of $\beta^0_0(22) = 0.7$. In the high J limit, a complete parallel orientation between $\mathbf{v}_{OH}$ and $\mathbf{J}_{OH}$ corresponds to a value of $\beta^0_0(22) = +1$. Since $\beta^0_0(22) = \langle P_2(\cos\theta_{tr}) \rangle$, the observed experimental value for $\beta^0_0(22)$ yields a narrow distribution for the angle between $\mathbf{v}_{OH}$ and $\mathbf{J}_{OH}$, $\theta_{tr} \cong 26°$.

E. $\langle \mu_{H_2O_2} \cdot \mathbf{v}_{OH} \cdot \mathbf{J}_{OH} \rangle$ correlation

The mutual correlation between the parent transition dipole moment $\mu_{H_2O_2}$ and the translational and rotational motion of the OH photoproduct is described by the bipolar moment $\beta^2_0(22)$.

In general, the θ,Φ dependence of $\beta^2_0(22)$ is given by

$$\beta^2_0(22) = -\tfrac{1}{8}\langle 2(1 - 3\cos^2\theta_t)(1 - 3\cos^2\theta_r) + 3\sin 2\theta_t \sin 2\theta_r \cos(\Phi_t - \Phi_r) - 6\sin^2\theta_t \sin^2\theta_r \cos 2(\Phi_t - \theta_r)\rangle. \quad (11)$$

The variation in $\beta^2_0(22)$ with the rotational quantum number N''_{OH} is small and within the experimental scatter as can be seen in Fig. 7(c). Since no correlation between $\mu_{H_2O_2}$ and $\mathbf{J}_{OH}$ as well as between $\mu_{H_2O_2}$ and $\mathbf{v}_{OH}$ is observed, a strong three vector correlation between $\mu_{H_2O_2}$, $\mathbf{v}_{OH}$, $\mathbf{J}_{OH}$ is also not expected, and the low value of the bipolar moment, $\beta^2_0(22) = 0.0 \pm 0.1$, is not surprising.

V. DISCUSSION

Four molecular singlet states, $\tilde{X}\,^1A$, $\tilde{A}\,^1A$, $\tilde{B}\,^1B$, $\tilde{C}\,^1A$, and four triplet states of hydrogen peroxide correlate with two ground state hydroxyl radicals, $X\,^2\Pi$. Except for the molecular ground state all states are repulsive. Since the oscillator strength for a transition from the electronic ground state, $\tilde{X}\,^1A\cdots 4a^2 5a^2 4b^2$, to one of the triplet states is several orders in magnitude lower than for a transition to a singlet state, only one bonding and three repulsive excited states correlating with two OH fragments are important in the UV photodissociation of hydrogen peroxide.[40]

Excitation of H_2O_2 at the long wavelength absorption end (248 and 266 nm) corresponds to a promotion of one of the two $4b$ electrons of the ground state to the lowest σ^* antibonding orbital of the $\tilde{A}\,^1A$ state. Since this is a $^1A \rightarrow {}^1A$ transition the dipole moment μ must be parallel to the C_2 symmetry axis, i.e., perpendicular to the O–O bond and thus perpendicular to the recoil direction of the fragments. Therefore, the bipolar moment $\beta^2_0(20)$ describing the translational anisotropy of the products must be -0.5 for an instantaneous fragmentation process. Any deviation from this value is caused by internal parent motion and finite time of separation for the fragmentation process. Indeed, a negative value of $\beta^2_0(20) = -0.36 \pm 0.05$ was found for the photodissociation of H_2O_2 at 266 nm indicating an upper limit for the molecular lifetime of 60 ps of hydrogen peroxide in the first electronic excited state, $\tilde{A}\,^1A$.[9]

If only the $\tilde{X}\,^1A \rightarrow \tilde{A}\,^1A$ transition is induced exclusively in the excitation process of hydrogen peroxide at 193 nm, then one should obtain a strong negative value for $\beta^2_0(20)$. A translational anisotropy parameter close to zero is observed [Fig. 7(a)] which can be explained only by a contribution of an additional transition to a state of ^1B geometry.

The transition dipole moment μ for a $^1A \rightarrow {}^1B$ transition has to lie perpendicular to the C_2 axis, but, in principle, may enclose any angle between 0° and 90° relative to the internuclear axis. However, an orientation of μ perpendicular to both, the C_2 axis and the O–O bond, results also in a strong negative value for $\beta^2_0(20)$. Therefore, the component of $\mu(^1A - {}^1B)$ perpendicular to the internuclear axis must be very small. *Ab initio* calculations[38] show that the second electronic excited $\tilde{B}$ state can be reached by raising one electron from the nonbonding $5a$ orbital to the $\tilde{B}\,^1B$ state. Since the ^1B state is reached by a $(\sigma_{00} \rightarrow \sigma^*_{00})$ transition, μ is aligned essentially parallel to the O–O bond. Chevaldonnet *et al.* have calculated the components of the transition moments between ground state and excited valence states ^1A and ^1B using a double-zeta basis set including polarization and Rydberg-type orbitals.[38] According to their calculation, the angle γ between the internuclear axis and μ is 20°. The expected anisotropy parameter $\beta^2_0(20)$ for an instantaneously dissociating molecule is then given by: $\beta^2_0(20) = P_2(\cos\gamma) = 0.82$.

In principle, even more than two electronic excited states could be responsible for the fragmentation process. However, higher states with ^1A symmetry demand a bipolar moment of $\beta^2_0(20) = -0.5$, and any contribution of these states to the overall dissociation process will be described by the symmetry of the $\tilde{A}\,^1A$ state. The same is valid for higher states with ^1B symmetry exhibiting a transition dipole moment essentially parallel to the O–O bond. These states contribute to the dissociation in the same manner as the $\tilde{B}\,^1B$ state. Only transitions to very high excited Rydberg states with ^1B symmetry could exhibit a dipole moment with a large angle to the internuclear axis. Furthermore, any other electronic excited singlet states ($\tilde{C},\tilde{D},\ldots$) are much higher in energy than the $\tilde{A}\,^1A$ and $\tilde{B}\,^1B$ states, and excitation with radiation at 193 nm becomes extremely unlikely. Reinsch calculated the components of the transition dipole moment for various electronic excited states in H_2O_2.[41] All transitions leading to a rupture of the O–O bond exhibit a dipole moment which is oriented either along the C_2 symmetry axis (for ^1A states) or essentially parallel to the internuclear axis (for ^1B states). Only transitions where OH* antibonding orbitals in H_2O_2 are excited exhibit a dipole moment with a large angle to the O–O axis. These electronic excited states correlate with a H atom and a HO_2 molecule. These products are not observed in the present study.[42]

The quantitative contribution of each fragmentation channel can be obtained from the observed bipolar moment $\beta^2_0(20)_{obs}$ and the bipolar moments $\beta^2_0(20)_A$ and $\beta^2_0(20)_B$ describing the c.m. angular distribution of products formed via repulsion on the $\tilde{A}\,^1A$ and on the $\tilde{B}\,^1B$ surface, respectively,

$$\beta^2_0(20)_{obs} = A\beta^2_0(20)_A + (1 - A)\beta^2_0(20)_B. \quad (12)$$

The quantities $\beta^2_0(20)_A$ and $\beta^2_0(20)_B$ are independent

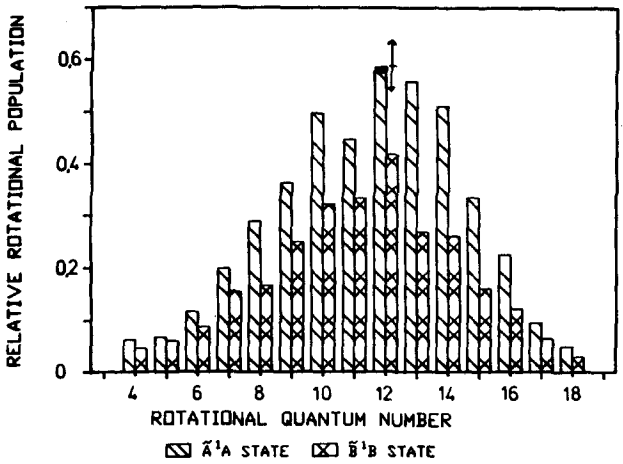

FIG. 8. Rotational state distribution of OH products after excitation of hydrogen peroxide in the $\tilde{A}\,^1A$ state (hatched bars) or in the $\tilde{B}\,^1B$ state (crosshatched bars). The black filled bar ($N''_{OH} = 12$) has to be added to the hatched bar of the $\tilde{A}\,^1A$ state if the parent dissociates instantaneously or to the crosshatched bar of the $\tilde{B}\,^1B$ state if the upper limit of 60 fs is taken for the fragmentation process. Experimental uncertainty is indicated by arrows at $N''_{OH} = 12$.

of the rotational state because they describe the correlation between the transition dipole moments, $\mu(\tilde{X}\,^1A\text{–}\tilde{A}\,^1A)$ or $\mu(\tilde{X}\,^1A\text{–}\tilde{B}\,^1B)$, of the parent H_2O_2 and the recoil velocity of the OH fragments. Since $\beta^2_0(20)_{obs}$ is obtained for each product quantum state, the microscopic differential cross section for each excited potential energy surface is determined.

Figure 8 shows the rotational state distribution of ejected OH photofragments after excitation of hydrogen peroxide at 193 nm in the $\tilde{A}\,^1A$ state (hatched bars) and in the $\tilde{B}\,^1A$ state (crosshatched bars), where $\beta^2_0(20)_{obs}$ is taken from Fig. 7. First a nonrotating hydrogen peroxide molecule which dissociates instantaneously, with $\beta^2_0(20)_A = -0.5$ and $\beta^2_0(20)_B = 0.82$, has been taken into account. Summing up the population of each rotational state separately for the $\tilde{A}$ and for the $\tilde{B}$ state, we find that 62% of the OH products are generated by ejection of the $\tilde{A}\,^1A$ electronic excited state, while 38% of the fragments are formed via the repulsion of the $\tilde{B}\,^1B$ state.

For a rotating parent molecule, the value of the parameters $\beta^2_0(20)_A$ and $\beta^2_0(20)_B$ are influenced by two effects. First, the recoil velocity v_r of the fragments can be effected by the tangential velocity v_t of the fragments during rotation of the parent. However, in the case of hydrogen peroxide, the axial velocity of O–O recoil is much higher than the tangential velocity, and the angle α by which the recoil direction is deflected by rotation of the parent is extremely small, $\alpha = \tan^{-1}(v_t/v_r) \simeq 3.6°$. Secondly, the $\beta^2_0(20)$ parameters will be influenced by the ratio of the lifetime τ of the excited H_2O_2 to its rotational period.

Several authors have given classical[27–29] and quantum mechanical[43] derivations of the influence of finite lifetime and parent rotation on the angular fragment distribution. According to the work of Bush and Wilson,[27] the parameter $\beta^2_0(20)_0$ is reduced by the factor f_{rot},

$$f_{rot} = \frac{P_2(\cos\alpha) + \omega^2\tau^2 - 3\omega\tau\sin\alpha\cos\alpha}{1 + 4\omega^2\tau^2}, \qquad (13)$$

$$\beta^2_0(20) = f_{rot}\,\beta^2_0(20)_0,$$

where ω describes the angular velocity of the parent and $\beta^2_0(20)_0$ is the bipolar moment for a nonrotating molecule which dissociates instantaneously after absorption of a photon. In the photodissociation of H_2O_2 at 266 nm, an upper limit of $\tau = 60$ fs was obtained for the lifetime of H_2O_2 in the $\tilde{A}\,^1A$ state.[28] At the shorter photolysis wavelength of 248 nm a limit of $\tau \leqslant 40$ fs was estimated for the dissociation to OH ($N''_{OH} = 1$).[11]

At 193 nm the lifetime of H_2O_2 in the electronic excited states is probably even shorter than 40 fs, because the fragments are formed with a higher recoil velocity. However, even the longer lifetime of $\tau = 60$ fs influences the relative contribution of the $\tilde{A}\,^1A$ and the $\tilde{B}\,^1B$ fragmentation channel to the overall dissociation process only to a minor extent.

The factor f_{rot} in Eq. (11) is calculated to be $f_{rot} = 0.85$ for $\tau = 60$ fs, and the values of the bipolar moments used in Eq. (10) become $\beta^2_0(20)_A = -0.43$ and $\beta^2_0(20)_B = 0.70$. The negligible influence of τ on the contribution of the $\tilde{A}\,^1A$ state is demonstrated in Fig. 8 for the case of the $N''_{OH} = 12$ rotational state. The small black filled bar has to be added to the crosshatched bar for $N''_{OH} = 12$ in order to take into account the finite parent lifetime in the electronic excited states.

In total, 62% of the OH products are formed on the $\tilde{A}\,^1A$ surface and 38% on the $\tilde{B}\,^1B$ surface when a H_2O_2 lifetime of 60 fs is assumed for both states. Thus, the correct value for the lifetime of hydrogen peroxide in the electronic excited states need not to be known to determine the contribution of the two separate dissociation channels.

Also, a variation in the orientation of the transition dipole moment connecting the ground state, $\tilde{X}\,^1A$, with the second excited state, $\tilde{B}\,^1B$, does not significantly change the calculated contribution of the two fragmentation channels. When $\mu(\tilde{X}\,^1A\text{–}\tilde{B}\,^1B)$ is exactly parallel to the O–O internuclear axis, then $\beta^2_0(20)_B$ becomes $\beta^2_0(20)_B = +1$, and one calculates that one third of the fragments are generated by ejection from the $\tilde{B}$ state.

The only quantity which markedly influences the calculated contribution of the two separate reaction channels is the measured bipolar moment $\beta^2_0(20)_{obs}$. The arrows in Fig. 8 indicate the maximum variation in the relative rotational state distribution caused by experimental scatter in determining $\beta^2_0(20)_{obs}$.

The c.m. angular distribution of ejected OH products formed in the rotational state $N''_{OH} = 12$ is shown in Fig. 9 in the form of a polar diagram. The observed total angular distribution $P(\theta)_{\tilde{A}+\tilde{B}}$ is the sum of both the $P(\theta)_{\tilde{A}}$ and $P(\theta)_{\tilde{B}}$ distributions generated after excitation of hydrogen peroxide in the $\tilde{A}\,^1A$ state and in the $\tilde{B}\,^1B$ state.

Since the observed bipolar moment $\beta^2_0(20)_{obs}$ (Fig. 7) is almost independent of the rotational state, the angular distributions of recoiled OH fragments generated in other states than $N''_{OH} = 12$ is comparable to the distribution shown in Fig. 9. The hatched region (Fig. 9) describes the uncertainty by finite lifetime of H_2O_2 in the upper electronic

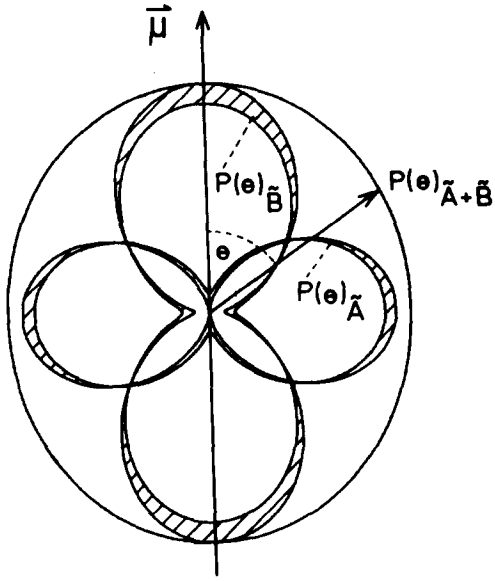

FIG. 9. Polar diagram of the c.m. angular distribution of ejected hydroxyl radicals formed in the rotational state $N''_{OH} = 12$ after excitation of hydrogen peroxide in the $\tilde{A}\,^1A$ state, $P(\theta)_{\tilde{A}}$, or in the $\tilde{B}\,^1B$ state, $P(\theta)_{\tilde{B}}$. The overall angular distribution, $P(\theta)_{\tilde{A}+\tilde{B}}$, is the sum of the individual distributions $P(\theta)_{\tilde{A}}$ and $P(\theta)_{\tilde{B}}$ for each angle θ. The hatched region describes the uncertainty by finite lifetime of H_2O_2 in the upper electronic states.

states. The dissociation time more strongly influences the angular distributions of OH photofragments than the relative contribution of each dissociation channel, because the angular distributions $P(\theta)_{\tilde{A}}$ and $P(\theta)_{\tilde{B}}$ are described by the parameters $\beta^2_0(20)_A$ and $\beta^2_0(20)_B$ which depend on the lifetime τ according to Eq. (11).

Both electronic excited states, ^1A and ^1B, are responsible for the rupture of the O–O bond in hydrogen peroxide at 193 nm leading to rotational excited OH products. The possible sources of this fragment rotation are parent molecule rotation, motion initially present as parent molecule vibration, a torque from an impulse along the recoil direction, and any torque generated by an angular dependence of the upper potential surfaces.

The rotation of the parent hydrogen peroxide makes only an extremely small contribution to the observed OH rotational excitation, because on the average only 80 cm^{-1} are transferred to OH rotation.[9] An impulse directed along the O–O internuclear axis would induce a torque on the O atoms in H_2O_2 which would be observable as OH rotation after the fragmentation.[44] This mechanism implies that 2.8% (1000 cm^{-1}) of the available energy (34 860 cm^{-1}) in the photofragmentation of H_2O_2 at 193 nm will appear as OH rotation. The rotational distribution should be sharply peaked around $N''_{OH} = 7$, and the rotational vector should be preferentially aligned perpendicular to $\mathbf{v}$. Since the observed $\langle \mathbf{v} \cdot \mathbf{J} \rangle$ correlation is strongly positive and the maximum of the rotational state distribution was found at $N''_{OH} = 12$, the main origin of the OH product rotation cannot be explained by an impulsive model.

The vibrational motion of the parent H_2O_2 may also be a source of OH product rotation. The ν_2 symmetric (1380 cm^{-1}) and ν_6 asymmetric (1266 cm^{-1}) bending modes as well as the ν_4 torsion mode can induce an angular momentum in the OH fragment. At room temperature, only the ν_4 internal torsion mode is vibrationally excited, and roughly 22% of all H_2O_2 parent molecules populate excited levels of the ν_4 mode.[9] The lowest energy level is 170 cm^{-1} above the potential minimum at a dihedral angle $\chi_m = 120°$.[45] The mean vibrational energy of ν_4 is calculated to be 255 cm^{-1} (including zero point energy). If no preferred absorption from vibrational excited levels take places, then the mean energy of the ν_4 mode and the zero point energies of both the ν_2 and ν_6 mode have to be distributed between the two OH fragments. The OH products can take almost half of this total vibrational energy as rotational energy.[46] Thus, each OH can receive 395 cm^{-1} (64 cm^{-1} from torsion and 331 cm^{-1} from bending motion) as rotational energy originating from the ν_2, ν_4, and ν_6 modes. A Gaussian distribution of parent vibrational momentum is transformed into a Gaussian rotational distribution of diatomic products.[47]

The OH rotation induced by the ν_4 mode of H_2O_2 will lead to an alignment of $\mathbf{J}_{OH}$ preferentially parallel to the recoil direction, and the bending motions will generate an OH rotation aligned perpendicular to $\mathbf{v}_{OH}$, because the OOH equilibrium angle θ is close to 90° ($\theta = 99°$).[45] We observe a much higher mean rotational energy ($\langle E_{rot} \rangle = 2780\ cm^{-1}$) and a strong positive correlation between $\mathbf{v}_{OH}$ and $\mathbf{J}_{OH}$. Therefore, the dominating part of OH product rotation originates from the torque provided by a strong dihedral angular dependence of both the $\tilde{A}\,^1A$ and the $\tilde{B}\,^1B$ state potentials.

For high OH rotations, quantum effects are less important, and a semiclassical momentum representation allows a more vivid physical interpretation. The values of the observed bipolar moments allow a determination of the expectation values $\langle J_x^2 \rangle$, $\langle J_y^2 \rangle$, and $\langle J_z^2 \rangle$ of the OH photofragment in the body-fixed axes of the H_2O_2 parent molecule. We define the z axis as the axis of the dipole moment $\boldsymbol{\mu}$ for both the transition to the $\tilde{A}\,^1A$ state as well as to the $\tilde{B}\,^1B$ state. The OH recoil velocity after excitation of the $\tilde{A}\,^1A$ state will be perpendicular to z and defines, e.g., the x axis. The bipolar moments describing the dissociation process are then connected with the expectation values of $\mathbf{J}_A$:

$$2J_A(J_A+1)\beta^2_0(02)_A = 2\langle J_z^2 \rangle_A - \langle J_x^2 \rangle_A - \langle J_y^2 \rangle_A, \tag{14}$$

$$2J_A(J_A+1)\beta^0_0(22)_A = 2\langle J_x^2 \rangle_A - \langle J_y^2 \rangle_A - \langle J_z^2 \rangle_A, \tag{15}$$

$$2J_A(J_A+1)\beta^2_0(22)_A = \langle J_x^2 \rangle_A + \langle J_z^2 \rangle_A - 2\langle J_y^2 \rangle_A. \tag{16}$$

The transition dipole moment connecting the H_2O_2 ground state with the $\tilde{B}\,^1B$ state lies almost parallel to the O–O bond. For a perfect parallel transition, the recoil velocity will be oriented parallel to $\boldsymbol{\mu}$, and the following relations hold:

$$2J_B(J_B+1)\beta^2_0(02)_B = 2\langle J_z^2 \rangle_B - \langle J_x^2 \rangle_B - \langle J_y^2 \rangle_B, \tag{17}$$

$$\beta^0_0(22)_B = -\beta^2_0(22)_B = \beta^2_0(02)_B. \tag{18}$$

Furthermore, the observed bipolar moments $\beta^k_0(k_1k_2)_{obs}$ are the sum of the corresponding bipolar moments of the $\tilde{A}$ and $\tilde{B}$ state:

$$\beta^{k}_{0}(k_1k_2)_{obs} = A\beta^{k}_{0}(k_1k_2)_{A} + (1-A)\beta^{k}_{0}(k_1k_2)_{B}. \quad (19)$$

Equations (12) to (19) are used to determine the bipolar moments $\beta^{k}_{0}(k_1k_2)_{A}$ and $\beta^{k}_{0}(k_1k_2)_{B}$ which describe the vector correlations in the fragmentation process of H_2O_2 at 193 nm when hydrogen peroxide is excited to the $\tilde{A}$ or to the $\tilde{B}$ state. The first row in Table II contains the observed bipolar moments at high OH rotational quantum numbers ($N''_{OH} > 14$) which are used to calculate the different vector correlations and expectation values $\langle J^2_x \rangle$, $\langle J^2_y \rangle$, and $\langle J^2_z \rangle$ for excitation of the $\tilde{A}\,^1A$ (row 2) and $\tilde{B}\,^1B$ state (row 3).

The bipolar moments $\beta^{0}_{0}(22)_{A}$ and $\beta^{0}_{0}(22)_{B}$ describing the correlation between $\mathbf{v}_{OH}$ and $\mathbf{J}_{OH}$ are both positive. Therefore, $\mathbf{v}_{OH}$ and $\mathbf{J}_{OH}$ are aligned more parallel to one another and both upper potential surfaces of H_2O_2 should exhibit a strong dependence on the torsion angle. Only a change in the torsion angle will cause a positive $\langle \mathbf{v}_{OH} \cdot \mathbf{J}_{OH} \rangle$ correlation. Any OH fragment motion along the bend coordinates will result in a more perpendicular orientation between $\mathbf{v}_{OH}$ and $\mathbf{J}_{OH}$. If this motion would dominate the fragmentation process, the bipolar moment $\beta^{0}_{0}(22)$ would be negative.

The expectation value $\langle J^2_x \rangle_A$ indicates that 80% of the OH rotational energy (after excitation of H_2O_2 to the $\tilde{A}\,^1A$ state) is induced by torsional motion while the remaining 20% result from bending motions. Excitation to the $\tilde{B}\,^1B$ state leads to similar results with slightly less rotational energy induced by the torsional motion. Since the ν_4 torsion mode of H_2O_2 in the ground state induces only a small angular momentum in the OH fragment, $\langle J^2_x \rangle_A$ and $\langle J^2_z \rangle_B$ are generated almost exclusively by a strong dependence on the dihedral angle of the upper potential surfaces.

The zero point energies of the ν_2 and ν_6 vibrational modes of the H_2O_2 parent ($330\,cm^{-1}$) contribute to a significant amount to the OH rotational energy originating from bending motions. Thus the upper potential surfaces should show a modest dependence along the symmetric and asymmetric bend coordinate. Since no vibrational excited OH photofragments are observed, the potential energy of both electronic excited states should be essentially independent on the OH stretch coordinate.

VI. CONCLUSION

In the current study our intention is to demonstrate how the mechanism of a photofragmentation process where different electronic excited states are involved can be elucidated by measuring the scalar and vectorial properties of the products, i.e., the internal state distribution, alignment, translation and correlations between the translational and internal motions of the OH fragment and the transition dipole moment of the parent H_2O_2. The individual contribution of the first two simultaneously excited singlet states to the overall dissociation process is obtained by determining various vector correlations using Doppler and polarization spectroscopy. When hydrogen peroxide is excited at 193 nm, most of the OH fragments are formed via the $\tilde{A}\,^1A$ state, and roughly one third of the products evolve from the $\tilde{B}\,^1B$ state. The OH product rotation mainly originates from the torque provided by the strong dihedral angular dependence of the $\tilde{A}\,^1A$ and $\tilde{B}\,^1B$ state potential. The analysis of the experimental data was supported by knowledge of the transition dipole moments in hydrogen peroxide. Measurements of the vector correlations as function of the excitation wavelength would indicate the beginning of another new transition induced in the parent molecule.

Although the current measurements give a direct and detailed insight into the final stage of the dissociation process, one important correlation has still to be determined: The correlation between the rotational angular momenta of both molecular fragments. This corresponds to a microscopic reaction probability for the formation of coincident product pairs. Since we observe a strong positive $\langle \mathbf{v} \cdot \mathbf{J} \rangle$ correlation which can only be caused by torsional motion, both OH products should be formed with similar rotation in the same elementary dissociation process, but the $\mathbf{J}_{OH}$ vectors pointing in opposite directions. Experiments are in progress in order to determine the correlation between coincident product pairs.

TABLE II. Bipolar moment $\beta^{k}_{0}(k_1k_2)$ and expectation values of the square of the angular momentum components. The transition dipole moment defines the z axis, and the recoiling OH fragments move along the x axis. The observed bipolar moments $\beta^{k}_{0}(k_1k_2)_{obs}$ were taken for high OH rotational quantum numbers to determine the vector correlations for excitation of the $\tilde{A}\,^1A$ and $\tilde{B}\,^1B$ state.

	$\beta^{2}_{0}(20)$	$\beta^{2}_{0}(02)$	$\beta^{0}_{0}(22)$	$\beta^{2}_{0}(22)$	$\langle J^2_x \rangle$	$\langle J^2_y \rangle$	$\langle J^2_z \rangle$
$\beta^{k}_{0}(k_1k_2)_{obs}$	−0.05	0.0	+0.70	0.0			
$\tilde{A}\,^1A$	−0.50	−0.37	+0.74	+0.37	0.82	0.09	0.09
$\tilde{B}\,^1B$	+1.0	+0.64	+0.64	−0.64	0.24		0.76

ACKNOWLEDGMENTS

The work has been performed as part of a program of the Deutsche Forschungsgemeinschaft. Financial support is gratefully acknowledged. We thank Professor E.-A. Reinsch [Frankfurt (Main)] for *ab initio* calculations on the H_2O_2 electronic states.

[1] S. R. Leone, Adv. Chem. Phys. **50**, 255 (1982).
[2] J. P. Simons, J. Phys. Chem. **88**, 1287 (1984).
[3] P. Andresen, G. S. Ondrey, B. Titze, and E. W. Rothe, J. Chem. Phys. **80**, 2548 (1984).
[4] R. Schinke, V. Engel, P. Andresen, D. Häusler, and G. G. Balint-Kurti, Phys. Rev. Lett. **55**, 1180 (1985).
[5] A. U. Grunewald, K.-H. Gericke, and F. J. Comes, Chem. Phys. Lett. **133**, 501 (1987).
[6] F. Alberti and A. E. Douglas, Chem. Phys. **34**, 399 (1978).
[7] A. M. Quinton and J. P. Simons, Chem. Phys. Lett. **81**, 214 (1981).
[8] R. Vasudev, R. N. Zare, and R. N. Dixon, Chem. Phys. Lett. **96**, 399 (1983); R. Vasudev, R. N. Zare, and R. N. Dixon, J. Chem. Phys. **80**, 4863 (1984).
[9] K.-H. Gericke, S. Klee, F. J. Comes, and R. N. Dixon, J. Chem. Phys. **85**, 4463 (1986); K.-H. Gericke, Faraday Discuss. Chem. Soc. **82**, 41 (1986).
[10] A. U. Grunewald, K.H. Gericke, and F. J. Comes, Chem. Phys. Lett. **132**, 121 (1986); F. J. Comes, Faraday Discuss. Chem. Soc. **82**, 43 (1986).
[11] M. P. Docker, A. Hodgson, and J. P. Simons, Chem. Phys. Lett. **128**, 264

(1986); Faraday Discuss. Chem. Soc. **82**, 25 (1986).
[12]M. Dubs, U. Brühlmann, and J. R. Huber, J. Chem. Phys. **84**, 3106 (1986).
[13]U. Brühlmann, M. Dubs, and J. R. Huber, J. Chem. Phys. **86**, 1249 (1986).
[14]O. Benoist d'Azy, F. Lahmani, V. Lardeux, and D. Solgadi, Chem. Phys. **94**, 247 (1985).
[15]R. Lavi, I. Bar, and S. Rosenwaks, J. Chem. Phys. **86**, 1639 (1987).
[16]M. Shapiro and R. Bersohn, Annu. Rev. Phys. Chem. **33**, 409 (1982).
[17]R. B. Bernstein, *Chemical Dynamics via Molecular Beam and Laser Technique* (Oxford University, New York, 1982).
[18]J. L. Kinsey, J. Chem. Phys. **66**, 2260 (1977).
[19]R. Schmiedl, H. Dugan, W. Meier, and K. H. Welge, Z. Phys. A **304**, 137 (1982).
[20]I. Nadler, D. Mahgerefteh, H. Reisler, and C. Wittig, J. Chem. Phys. **82**, 3885 (1985).
[21]R. Schinke, J. Phys. Chem. **90**, 1742 (1986).
[22]R. N. Zare and D. R. Herschbach, Proc. IEEE **51**, 173 (1963).
[23]R. Bersohn and S. H. Lin, Adv. Chem. Phys. **16**, 67 (1964).
[24]C. H. Greene and R. N. Zare, Annu. Rev. Phys. Chem. **33**, 119 (1982); J. Chem. Phys. **78**, 6741 (1983).
[25]U. Fano and J. H. Macek, Rev. Mod. Phys. **45**, 553 (1973).
[26]D. A. Case, G. M.McClelland, and D. R. Herschbach, Mol. Phys. **35**, 541 (1978).
[27]G. E. Bush and K. R. Wilson, J. Chem. Phys. **56**, 3638, 3655 (1972).
[28]S. Klee, K.-H. Gericke, and F. J. Comes, J. Chem. Phys. **85**, 40 (1986).
[29]J. Solomon, C. Jonah, P. Chandra, and R. Bersohn, J. Chem. Phys. **55**, 1908 (1971); C. Jonah, *ibid.* **55**, 1915 (1971).
[30]T. Nagata, T. Kondow, K. Kuchitsu, G. W. Loge, and R. N. Zare, J. Mol. Phys. **50**, 49 (1983).
[31]G. E. Hall, N. Sivakumar, P. L. Houston, I. Burak, Phys. Rev. Lett. **56**, 1671 (1986).
[32]G. E. Hall, N. Sivakumar, R. Ogorzalek, G. Chawla, H.-P. Haerri, P. L. Houston, I. Burak, and J. W. Hepburn, Faraday Discuss. Chem. Soc. **82**, 1 (1986).
[33]R. N. Dixon, J. Chem. Phys. **85**, 1866 (1986).
[34]I. Burak, J. W. Hepburn, N. Sivakumar, G. E. Hall, G. Chawla, and P. L. Houston, J. Chem. Phys. **86**, 1258 (1987).
[35]J. P. Simons, A. J. Smith, Chem. Phys. Lett. **97**, 1 (1983).
[36]H. Gölzenleuchter, K.-H. Gericke, and F. J. Comes (to be published).
[37]M. Suto and L. C. Lee, Chem. Phys. Lett. **98**, 152 (1983); L. T.Molina and M. J. Molina, J. Photochem. **15**, 97 (1981).
[38]C. Chevaldonnet, H. Cardy, and A. Dargelos, Chem. Phys. **102**, 55 (1986).
[39]G. Ondrey, N. van Veen, and R. Bersohn, J. Chem. Phys. **78**, 3732 (1983).
[40]E. M. Evleth, J. Am. Chem. Soc. **98**, 1637 (1976); E. M. Evleth and E. Kassab, J. Am. Chem. Soc. **100**, 7859 (1978).
[41]E. A. Reinsch, Frankfurt (private communication).
[42]U. Gerlach-Meyer, E. Linnebach, K. Kleinermanns, and J. Wolfrum, Chem. Phys. Lett. **133**, 113 (1987).
[43]S. Yang and R. Bersohn, J. Chem. Phys. **61**, 4400 (1974).
[44]A. F. Tuck, Trans. Faraday Soc. **73**, 689 (1977).
[45]The structure parameters of H_2O_2 have been analyzed in different papers using microwave data. D. Cremer, J. Chem. Phys. **69**, 4440 (1978) showed that the evaluation of several parameters was not completely error free. We adopt the parameters of the work of Cremer and Christen which were obtained by a reanalysis of all existing H_2O_2 microwave spectra: G. A. Kachkuruzov, and I. N. Przhevalskii, Opt. Spectrosc. **36**, 172 (1974); D. Cremer and D. Christen, J. Mol. Spectrosc. **74**, 480 (1979).
[46]H. Gölzenleuchter, K.-H. Gericke, F. J. Comes, and P. F. Linde, Chem. Phys. **89**, 93 (1984).
[47]M. D. Morse and K. F. Freed, J. Chem. Phys. **78**, 6045 (1983); M. D. Morse, Y. B. Band, and K. F. Freed, *ibid.* **78**, 6066 (1983).